The Astrophysical Journal, 790:14 (7pp), 2014 July 20 doi:10.1088/0004-637X/790/1/14

MOA-2013-BLG-220Lb: MASSIVE PLANETARY COMPANION TO GALACTIC-DISK HOST

J. C. Yee[1,2,39,40], C. Han[3,40,41], A. Gould[1,40], J. Skowron[4,42], I. A. Bond[5,43], A. Udalski[4,43], M. Hundertmark[6,44], L. A. G. Monard[7,40], I. Porritt[8,40], P. Nelson[9,40], V. Bozza[10,11],
and
M. D. Albrow[12], J.-Y. Choi[3], G. W. Christie[13], D. L. DePoy[14], B. S. Gaudi[1], K.-H. Hwang[3], Y. K. Jung[3], C.-U. Lee[15], J. McCormick[16], T. Natusch[13,17], H. Ngan[13], H. Park[3], R. W. Pogge[1], I.-G. Shin[3], T.-G. Tan[18]
(The μFUN Collaboration),
F. Abe[19], D. P. Bennett[20], C. S. Botzler[21], M. Freeman[21], A. Fukui[22], D. Fukunaga[19], Y. Itow[19], N. Koshimoto[23], P. Larsen[24], C. H. Ling[5], K. Masuda[19], Y. Matsubara[19], Y. Muraki[19], S. Namba[23], K. Ohnishi[25], L. Philpott[26], N. J. Rattenbury[21], To. Saito[27], D. J. Sullivan[28], T. Sumi[23], W. L. Sweatman[5], D. Suzuki[23], P. J. Tristram[29], N. Tsurumi[19], K. Wada[23], N. Yamai[30], P. C. M. Yock[21], A. Yonehara[30]
(MOA Collaboration),
M. K. Szymański[4], K. Ulaczyk[4], S. Kozłowski[4], R. Poleski[1,4], Ł. Wyrzykowski[4,24], M. Kubiak[4], P. Pietrukowicz[4], G. Pietrzyński[4,31], I. Soszyński[4]
(OGLE Collaboration),
D. M. Bramich[32], P. Browne[6], R. Figuera Jaimes[6,33], K. Horne[6], S. Ipatov[34], N. Kains[33], C. Snodgrass[35], I. A. Steele[36], R. Street[37], Y. Tsapras[37,38]
(The RoboNet Collaboration),
[1] Department of Astronomy, Ohio State University, 140 West 18th Avenue, Columbus, OH 43210, USA
[2] Harvard-Smithsonian Center for Astrophysics, 60 Garden Street, Cambridge, MA 02138, USA
[3] Department of Physics, Chungbuk National University, Cheongju 361-763, Korea
[4] Warsaw University Observatory, Al. Ujazdowskie 4, 00-478 Warszawa, Poland
[5] Institute of Information and Mathematical Sciences, Massey University, Private Bag 102-904, North Shore Mail Centre, Auckland, New Zealand
[6] SUPA, School of Physics and Astronomy, University of St Andrews, North Haugh, St Andrews KY16 9SS, UK
[7] Klein Karoo Observatory, Centre for Backyard Astrophysics, Calitzdorp, South Africa
[8] Turitea Observatory, Palmerston North, New Zealand
[9] Ellinbank Observatory, Ellinbank, Victoria, Australia
[10] Dipartimento di Fisica "E. R. Caianiello," Università degli Studi di Salerno, Via S. Allende, I-84081 Baronissi (SA), Italy
[11] Instituto Nazionale di Fisica Nucleare, I-80126 Sezione di Napoli, Italy
[12] Department of Physics and Astronomy, University of Canterbury, Private Bag 4800, Christchurch 8020, New Zealand
[13] Auckland Observatory, Auckland, New Zealand
[14] Department of Physics and Astronomy, Texas A&M University, College Station, TX 77843-4242, USA
[15] Korea Astronomy and Space Science Institute, 776 Daedukdae-ro, Yuseong-gu, Daejeon 305-348, Korea
[16] Farm Cove Observatory, Centre for Backyard Astrophysics, Pakuranga, Auckland, New Zealand
[17] Institute for Radio Astronomy and Space Research, AUT University, Auckland, New Zealand
[18] Perth Exoplanet Survey Telescope, Perth, Australia
[19] Solar-Terrestrial Environment Laboratory, Nagoya University, Nagoya 464-8601, Japan
[20] Department of Physics, University of Notre Dame, 225 Nieuwland Science Hall, Notre Dame, IN 46556-5670, USA
[21] Department of Physics, University of Auckland, Private Bag 92-019, Auckland 1001, New Zealand
[22] Okayama Astrophysical Observatory, National Astronomical Observatory of Japan, Asakuchi, Okayama 719-0232, Japan
[23] Department of Earth and Space Science, Osaka University, Osaka 560-0043, Japan
[24] Institute of Astronomy, University of Cambridge, Madingley Road, Cambridge CB3 0HA, UK
[25] Nagano National College of Technology, Nagano 381-8550, Japan
[26] Department of Physics and Astronomy, The University of British Columbia, 6224 Agricultural Road, Vancouver, BC V6T 1Z1, Canada
[27] Tokyo Metropolitan College of Aeronautics, Tokyo 116-8523, Japan
[28] School of Chemical and Physical Sciences, Victoria University, Wellington, New Zealand
[29] Mt. John University Observatory, P.O. Box 56, Lake Tekapo 8770, New Zealand
[30] Department of Physics, Faculty of Science, Kyoto Sangyo University, 603-8555 Kyoto, Japan
[31] Departamento de Astronomia, Universidad de Concepción, Casilla 160-C, Concepción, Chile
[32] Qatar Environment and Energy Research Institute, Qatar Foundation, Tornado Tower, Floor 19, P.O. Box 5825, Doha, Qatar
[33] European Southern Observatory, Karl-Schwarzschild-Str. 2, D-85748 Garching bei München, Germany
[34] Qatar Foundation, P.O. Box 5825, Doha, Qatar
[35] Max Planck Institute for Solar System Research, Max-Planck-Str. 2, D-37191 Katlenburg-Lindau, Germany
[36] Astrophysics Research Institute, Liverpool John Moores University, Liverpool CH41 1LD, UK
[37] Las Cumbres Observatory Global Telescope Network, 6740 Cortona Drive, Suite 102, Goleta, CA 93117, USA
[38] School of Physics and Astronomy, Queen Mary University of London, Mile End Road, London E1 4NS, UK
Received 2014 March 9; accepted 2014 May 28; published 2014 June 27

ABSTRACT

We report the discovery of MOA-2013-BLG-220Lb, which has a super-Jupiter mass ratio $q = 3.01 \pm 0.02 \times 10^{-3}$ relative to its host. The proper motion, $\mu = 12.5 \pm 1\,\mathrm{mas\,yr^{-1}}$, is one of the highest for microlensing planets yet discovered, implying that it will be possible to separately resolve the host within ~7 yr. Two separate lines of evidence imply that the planet and host are in the Galactic disk. The planet could have been detected and

characterized purely with follow-up data, which has important implications for microlensing surveys, both current and into the Large Synoptic Survey Telescope (LSST) era.

Key words: gravitational lensing: micro – planetary systems

Online-only material: color figures

1. INTRODUCTION

Because microlensing planet detections are based on observations of a background source that is lensed by the planetary system, rather than observations of the planetary system itself, microlensing is unique in its ability to detect planets orbiting extremely dim or dark hosts or even planets without hosts (Sumi et al. 2011). For the same reason, however, microlensing planet hosts are often difficult to characterize. This can in principle be done by simultaneously measuring two higher-order effects during the event, yielding the Einstein radius $\theta_{\rm E}$ and the "microlens parallax" $\pi_{\rm E}$. Then the lens mass M and lens–source relative parallax $\pi_{\rm rel}$ are given by (Gould 1992)

$$M = \frac{\theta_{\rm E}}{\kappa \pi_{\rm E}}; \quad \pi_{\rm rel} = \pi_{\rm E}\theta_{\rm E}; \quad \kappa \equiv \frac{4G}{c^2\,{\rm AU}} \simeq 8.1\,\frac{\rm mas}{M_\odot}. \quad (1)$$

This has been successfully carried out for a significant minority of microlensing planets to date and actually verified in one case by direct imaging (Gaudi et al. 2008; Bennett et al. 2010). However, while $\theta_{\rm E}$ has been measured in the great majority of published planetary events, $\pi_{\rm E}$ usually proves too difficult to measure. In this case, one only has the mass–distance constraint

$$M\pi_{\rm rel} = \frac{\theta_{\rm E}^2}{\kappa}. \quad (2)$$

An alternate approach is to directly observe the lens in high-resolution images, either under the "glare" of the source while they are still superposed, provided that the lens is sufficiently bright (Batista et al. 2014), or by waiting for the lens and source to separate (V. Batista et al. 2014, in preparation; D. P. Bennett et al. 2014, in preparation). Of course, direct imaging is ill-suited to detecting dark hosts, but it can at least verify that they are dark, particularly if the mass–distance constraint (Equation (2)) is available.

Here we present MOA-2013-BLG-220Lb with super-Jupiter planet/host mass ratio $q = 3.0 \times 10^{-3}$. Although the host (and so planet) mass is presently unknown, we show that it is moving rapidly away from the source ($\mu_{\rm rel} = 12.5 \pm 1$ mas yr^{-1}) and so can be imaged separately within ~7 yr.

2. OBSERVATIONS

On 2013 April 1, UT 19:08, the Microlensing Observations in Astrophysics (MOA) Collaboration[45] issued an alert that MOA-2013-BLG-220 was an ongoing microlensing event at (R.A., decl.)= (18 : 03 : 56.5, −29 : 32 : 41), (l, b) = (1.50, −3.76), based on data taken in a broad RI band using their 1.8 m telescope at Mt. John, New Zealand. μFUN issued its own alert 46 hr later saying that this was likely to be a high-magnification event and thus very sensitive to planets (Griest & Safizadeh 1998), which triggered observations by the Kleinkaroo Observatory. These data showed a sharp increase in brightness, which was interpreted as evidence of a very high magnification event and so triggered a further alert, but was actually due to the onset of the anomaly (see Figure 1). This alert, issued as the event was rising over Chile, noted that μFUN's own telescope at that location was nonoperational due to equipment problems and made a particular request that other telescopes at this longitude observe the event.

The Optical Gravitational Lens Experiment (OGLE) responded by putting their 1.3 m telescope at Las Campanas, Chile, which is usually dedicated to microlensing survey operations, into "follow-up mode." Specifically, OGLE found that MOA-2013-BLG-220 lay in a gap between OGLE mosaic-camera CCD chips in the template image of this field. Thus, although they did have occasional observations of this target when the telescope pointing drifted slightly, they were not monitoring these observations in real time and so did not issue an alert. However, in response to μFUN's alert, OGLE both slightly changed the pointing of their telescope for this survey field and also dramatically increased the cadence. It is not uncommon for OGLE to increase cadence in response to interesting events (e.g., Yee et al. 2012), but altered pointing is much rarer.

The OGLE follow-up data showed a clear caustic exit, which was the first unambiguous evidence for a planetary (or possibly binary) event. This triggered a further alert. In the end, follow-up data were taken by seven μFUN telescopes, three RoboNet telescopes, one follow-up telescope on the same site as the MOA survey telescope, and OGLE in follow-up mode.

The seven μFUN sites are Kleinkaroo Observatory (30 cm unfiltered, Calitzdorp, South Africa), Turitea Observatory (36 cm R band, Palmerston, New Zealand), Ellinbank Observatory (32 cm V band, Victoria, Australia), PEST Observatory (30 cm, unfiltered, Perth, Australia), Auckland Observatory (40 cm R band, Auckland, New Zealand), Farm Cove Observatory (36 cm unfiltered, Pakuranga, New Zealand), and CTIO SMARTS (1.3 m I, V bands, La Serena, Chile), with all but the last being amateur observatories.

All three RoboNet telescopes are 1 m and robotic, with one at La Serena, Chile (I band, CTIO-LCOGT) and two at Sutherland, South Africa (I band, SAAO-LCOGT-B,C). In particular, the data from Chile covered the second caustic exit extremely well.

The MOA 61 cm B&C telescope (I band, Mt. John, New Zealand) responded to the alert by obtaining intensive observations over the next two nights, in particular tracing a subtle structure of the second caustic exit.

All data were reduced using difference image analysis (Alard & Lupton 1998; Bramich 2008).

3. LIGHTCURVE ANALYSIS

3.1. Topological Analysis

Figure 1 shows the data together with the best-fit model. However, the basic character of the event can be understood

[39] Sagan Fellow.
[40] The μFUN Collaboration.
[41] Corresponding author.
[42] The OGLE Collaboration.
[43] The MOA Collaboration.
[44] The RoboNet Collaboration.
[45] https://it019909.massey.ac.nz/moa/

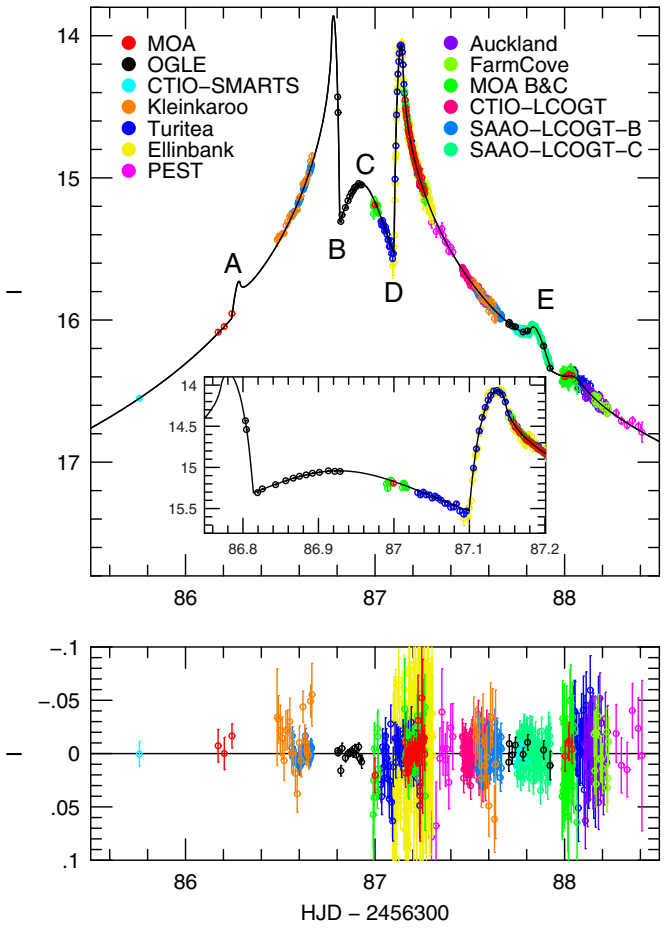

Figure 1. Best-fit model and residuals for MOA-2013-BLG-220. From the lightcurve alone, it is clear that there are two caustic crossings (ending at ∼86.8 (B) and starting at ∼87.1 (D)) and a cusp approach (∼86.95 (C)), hence three cusps on one side of the primary lens, implying a planetary mass ratio for the companion. The fact that the time (∼0.15 day) from the cusp approach (C) to second entrance (D) is much shorter than the time (∼0.85 day) to the second exit (E) shows that the caustic has a resonant topology, implying $|s - 1| \ll 1$. See Figure 2. The near symmetry of the lightcurve about the cusp approach implies that the source passed nearly perpendicular to the planet–star axis. All of these predictions are confirmed by detailed modeling. See Table 1. Kleinkaroo and PEST data are binned for plotting purposes but are not binned in the lightcurve fitting.

(A color version of this figure is available in the online journal.)

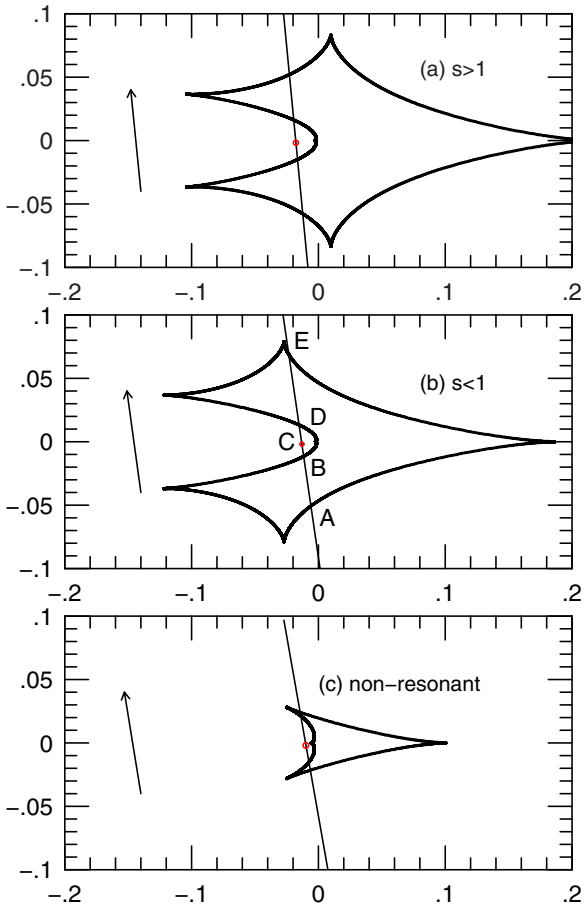

Figure 2. Three possible central caustic topologies that could be consistent with the lightcurve in Figure 1; (a) and (b) resonant six-sided caustic with $s > 1$ ($s < 1$) and (c) nonresonant four-sided caustic (same for both $s > 1$ and $s < 1$). The trajectory must pass roughly perpendicular to the caustic axis, close to the central cusp (as shown) in order to reproduce the lightcurve's approximate symmetry. The fact that the time from the cusp approach (C) to the second entrance (D) is much shorter than from cusp approach (C) to the second exit (E) rules out topology (c). Topology (b) is preferred over (a) by $\Delta\chi^2 \sim 6000$. This preference is not easily traceable to gross features of the lightcurve, but see Section 3 for qualitative reasoning. The caustic geometries in (a) and (b) correspond to the actual best-fit solutions for the indicated topologies.

(A color version of this figure is available in the online journal.)

without reference to any model. The first feature is that the peak magnification is $A_{\rm max} \gtrsim 100$, just from comparison of the peak and baseline flux ($I_{\rm base} \sim 19.0$, not shown). This implies that the strong perturbations are due to a central caustic probing normalized lens–source separation $u \ll 1$ (since $A \sim u^{-1}$).

The OGLE data and Turitea and Ellinbank data show clear caustic exit (B) and entry (D), respectively. In between, there is a clear "bump" (C), which is characteristic of a cusp crossing or cusp approach. These features already tell us that there are three cusps on one side of the primary lens, which by itself implies that the caustic has one of the three topologies shown in Figure 2: resonant (six-sided) caustic for lens–companion separation $s > 1$ (normalized to $\theta_{\rm E}$), resonant caustic for $s < 1$ (both with $|s - 1| \ll 1$), or nonresonant (four-sided) caustic (same for $s > 1$ or $s < 1$). The fact that the lightcurve is roughly symmetric about the central bump shows that the trajectory passed roughly perpendicular to the primary-companion axis. See Figure 2. The caustic exit, traced by OGLE, CTIO, and MOA B&C data (E) then clearly favors the resonant topologies over the central caustic. This is because the time from the bump midpoint (C) to the caustic re-entrance (D) is very short compared to the time from re-entrance (D) to final exit (E). This accords well with the resonant topologies but clearly contradicts the nonresonant topology. The fact that the caustic is both small and resonant already tells us that this is a planetary event $q \lesssim 0.01$. That is, roughly equal mass binaries can produce small caustics if $s \gg 1$ or $s \ll 1$, but in this case they are nonresonant, roughly equilateral, four-sided caustics.

The fact that the resonant caustic has a "close" ($s < 1$) rather than "wide" ($s > 1$) topology is not easily discerned by eye, but it can be understood qualitatively with the help of Figures 1 and 2. First, the fact that the Turitea–Ellinbank caustic entrance (D) is slightly lower than the OGLE caustic exit (B) in Figure 1 tells us that the source was further from the center of magnification. Therefore, it was not moving quite perpendicular to the star–planet axis, but rather slightly to the left in Figure 2.

Note that for the wide topology, the top and bottom cusps are to the right of the central cusp, while for the close topology they are to the left. The reason for this difference is deeply rooted in the nature of planetary lensing. For $s > 1$, as s further increases, these outward cusps will move further to the right (toward the position of the planet) and eventually break off to form a quadrilateral caustic on the same side as the planet. By contrast, for $s < 1$ as s further decreases, the outward cusps will move to the left and eventually break off to form two triangular caustics on the opposite side of the planet. This asymmetry reflects the fact that a point lens has two images: one outside the Einstein ring on the same side as the source, and one inside the Einstein ring on the opposite side. In the planetary ($q \ll 1$) limit, the planet betrays its presence by perturbing one of these two images. A planet outside the Einstein ring ($s > 1$) must perturb the first, and hence the image must be on the same side as the planet, while for $s < 1$ it must be on the opposite side of the planet.[46]

Hence, the "tilt" of the trajectory implies that it is headed near the outward cusp (E) in the close topology and away from the cusp in the wide topology. This implies a much longer delay until the caustic exit for the close topology. See Figure 2. The model in Figure 1 shows that the time from first caustic entrance (86.2, (A)) to central cusp passage (86.9, (C)) is substantially shorter than from central cusp (C) to second caustic exit (87.8, (E)), consistent with a close topology. Unfortunately, the coverage of the first caustic entrance (A) is not complete enough to securely identify it without the aid of a model. Hence, full modeling is required to finally determine that $s < 1$ is the correct topology. In fact, the wide topology is rejected at $\Delta\chi^2 \sim 6000$.

3.2. Mathematical Model

We model the lightcurve using Stokes' method (Gould & Gaucherel 1997) for highly perturbed regions of the lightcurve and hexadecapole (Pejcha & Heyrovský 2009; Gould 2008) for the moderately perturbed regions. To account for limb darkening, we use a linear limb-darkening law and model the source as $n = 10$ annuli for the Stokes integration (after testing that $n = 20$ yields essentially the same results) and use the prescription of Gould (2008) for hexadecapole. We derive coefficients $(u_V, u_R, u_I) = (0.6504, 0.5756, 0.4955)$ from Claret (2000) using $T_{\rm eff} = 6125$ K and $\log g = 4.0$, based on the measured color $(V-I)_0 = 0.585$ and the inferred source radius $R_* \simeq R_0\theta_* = 1.25\,R_\odot$ (see Section 4). These correspond to $(\Gamma_V, \Gamma_R, \Gamma_I) = (0.554, 0.475, 0.396)$.

Table 1 shows the resulting microlensing fit parameters. Here, $(u_0, t_0, t_{\rm E})$ are the parameters of the underlying event, respectively the impact parameter (normalized to $\theta_{\rm E}$) of the source trajectory relative to the center of magnification of the lens system, the time of closest approach, and the Einstein radius crossing time. The planet parameters are (s, q, α), respectively the normalized planet–host separation, the planet–host mass ratio, and the angle of the planet–host axis relative to the source trajectory. Finally, $\rho \equiv \theta_*/\theta_{\rm E}$ is the normalized source radius, while f_s and f_b are the fluxes due to the lensed source and the unlensed blended light in the aperture, respectively.

[46] In the strict planetary limit, $q \to 0$, the outer cusps are perfectly aligned with the central cusp at $s = 1$, but for finite q (and $s = 1$) the outer cusps lie increasingly to the right of the central cusp and only "pass" it at roughly $s_{\rm vertical} \sim 1$–$0.55q$. In the present case, the planetary limit applies, but in general one should be aware of this effect.

Table 1
Microlens Parameters

Parameter	Value	Error
$t_0 - 6386$	0.9199	0.0009
$u_0 \times 10^3$	13.23	0.04
$t_{\rm E}$(days)	13.23	0.05
$\rho \times 10^3$	1.54	0.01
s	0.9857	0.0001
$q \times 10^3$	3.01	0.02
α (deg)	261.5	0.2
I_s (OGLE)	19.205	0.003
f_b/f_s (OGLE)	0.175	0.004
$\theta_{\rm E}$ (mas)[a]	0.456	0.003
$\mu_{\rm geo}$ (mas yr^{-1})[a]	12.57	0.08

Note. [a] Error shown is from lightcurve only. Additional 7% systematic error is discussed in the text.

4. PHYSICAL PARAMETERS

4.1. Angular Scale

The source crossing time, $t_* = \rho t_{\rm E} = 29$ minutes, is exceptionally short for microlensing events, indicating either a high proper motion or very small source. From regression of CTIO-SMARTS V/I data, we derive a model-independent instrumental source color $(V-I)_{s,\rm inst} = -0.39$, and from the model we obtain $I_{s,\rm inst} = 19.46$. We measure the instrumental position of the clump as $(V-I, I)_{\rm cl,inst} = (0.07, 15.94)$ and adopt $(V-I, I)_{0,\rm cl} = (1.06, 14.39)$ from Bensby et al. (2013) and Nataf et al. (2013), and so derive $(V-I, I)_{0,s} = (0.60, 18.04)$. Using a similar procedure for OGLE V/I data, we infer $(V-I, I)_{0,s} = (0.57, 17.91)$. We adopt the average of these. Using the *VIK* color–color relations of Bessell & Brett (1988) and the color/surface-brightness relations of Kervella et al. (2004), we find $\theta_* = 0.704\,\mu$as. We then find

$$\mu_{\rm geo} = \frac{\theta_*}{t_*} = 12.5\,{\rm mas\,yr^{-1}}; \quad \theta_{\rm E} = \frac{\theta_*}{\rho} = 0.45\,{\rm mas}, \qquad (3)$$

where $\mu_{\rm geo}$ is the instantaneous lens–source relative proper motion in the geocentric frame at the peak of the event. The principal errors in these quantities derive from the color–magnitude offset of the source from the clump, rather than the microlensing fit parameters $(t_{\rm E}, \rho, I_s)$. The color error is known from spectroscopy of a microlensing subsample to be 0.05 mag (Bensby et al. 2013).[47] We estimate the magnitude error, which is basically due to uncertainty in centroiding the clump, to be 0.10 mag. This value is consistent with general practice and also with the difference between the CTIO-SMARTS-based and OGLE-based determinations. In principle, one might adopt an error that is smaller by $\sqrt{2}$ due to averaging two determinations, but we conservatively decline to do so. Combined, these yield a fractional error in θ_* of 7%, which then propagates directly to uncertainties in μ and $\theta_{\rm E}$.

[47] The overall scatter between $(V-I)_0$ as inferred from microlensing color (i.e., the method used here) and from spectroscopy in the Bensby et al. (2013) sample is about 0.07 mag. However, as those authors discuss, this scatter is dominated by relatively red sources, for which the most likely cause is errors in the photospheric models. Hence, it is more appropriate to adopt a smaller uncertainty for bluer sources like MOA-2013-BLG-220. In addition, roughly 0.03 mag of the scatter (in quadrature) is caused by measurement error in the spectroscopic temperature.

4.2. Mass–Distance Constraint

This measurement of θ_E directly relates the lens mass and distance via Equation (2)

$$M\pi_{\rm rel} = \frac{\theta_E^2}{\kappa} = 0.025\,M_\odot\,{\rm mas}. \quad (4)$$

If the lens were in or near the bulge, then $M \simeq 1.7\,M_\odot\,({\rm kpc}/D_{LS})$, where $D_{LS} = D_S - D_L$ is the distance between the lens and source. However, unless the lens is a black hole or neutron star, it must be $M < 1\,M_\odot$. This is because the source has $M_I \sim 3.4$, and the lens (which is closer) must be at least ∼1 mag dimmer or it would be seen in the blended light. Therefore, the lens must be more than 1.7 kpc in front of the source ($D_L < 6.5\,{\rm kpc}$, $M < 0.77\,M_\odot$) and so almost certainly in the Galactic disk.

Because Turitea and Ellinbank observatories are separated by about 2500 km and both cover the caustic entrance, which is a very sharp feature in the lightcurve, it is in principle possible to measure the "microlens parallax" vector $\boldsymbol{\pi}_E = (\pi_{E,{\rm North}}, \pi_{E,{\rm East}})$ (Gould 2004; Hardy & Walker 1995; Gould et al. 2009) from the lightcurve differences (after taking account of limb-darkening differences). Even a very weak constraint would be of some interest. For example if $\pi_E < 3$, then the lens–source relative parallax would be $\pi_{\rm rel} = \theta_E\pi_E < 1.3$, meaning that the lens would be further than 700 pc. Unfortunately, we find no meaningful constraints at the 3σ level.

5. SOURCE–LENS RELATIVE PROPER MOTION

The high proper motion in Equation (3) should be compared to our expectation for typical lens–source relative proper motions. A typical proper motion for a lens in the bulge is $\mu \sim 4\,{\rm mas\,yr^{-1}}$ and for a disk lens, $\mu \sim \mu_{\rm sgrA*} = 6.4\,{\rm mas\,yr^{-1}}$. The former is due to typical one-dimensional lens and source dispersions of $\sim 100\,{\rm km\,s^{-1}}$ at Galactocentric distance $R_0 \sim 8.2\,{\rm kpc}$ while the latter is due to the Sun and the lens partaking of the same approximately flat Galactic rotation curve.

There are two basic ways to produce higher proper motions: either lenses and/or sources that are moving very fast relative to their populations, or nearby lenses. In the latter case, we expect that the typical peculiar motions of stars relative to their local LSR, $v_{\rm pec} \sim 30\,{\rm km\,s^{-1}}$ will add as a more-or-less randomly oriented vector $\Delta\mu = v_{\rm pec}/D_L \sim 6\,{\rm mas\,yr^{-1}}({\rm kpc}/D_L)$. Hence, if this is the cause, one expects that the lens will be within a few kiloparsec.

While the MOA-2013-BLG-220 "source star" (actually, "baseline object") mostly fell between chips in the OGLE-IV survey, it was observed 1298 times between 2001 and 2009 by OGLE-III. We are therefore able to measure its proper motion (relative to a frame of Galactic bulge stars):

$$\boldsymbol{\mu}_{\rm base} = (\mu_\ell, \mu_b) = (-5.6, +1.9)\,{\rm mas\,yr^{-1}} \quad (5)$$

with an error of $1.2\,{\rm mas\,yr^{-1}}$ in each direction. That is, the baseline object is moving almost directly opposite to the direction of Galactic rotation.

However, the light in the baseline object may also include light from stars other than the source. Hence, while the source dominates the light from the baseline object, a minority of the light may be coming from the lens or some other unrelated object. Nominally, our measurement indicates that 15% of the baseline flux, $f_{\rm base} = f_s + f_b$, comes from the blended light (f_b) rather than from the source (f_s). However, this may be because the estimate of the baseline flux is itself the result of crowded-field photometry (DoPHOT; Schechter et al. 1993), rather than difference imaging and so is subject to considerable uncertainty. If this ($f_b/f_{\rm base}$) estimate were by chance perfectly accurate and if, for example, the blended light is not moving in the bulge frame, then $\mu_s = \mu_{\rm base} f_{\rm base}/f_s = 7.2\,{\rm mas\,yr^{-1}}$. Hence, the $\boldsymbol{\mu}_{\rm base}$ measurement is a strong qualitative indication of source motion, though not a direct determination of it. Nevertheless, if we adopt $\boldsymbol{\mu}_s \sim \boldsymbol{\mu}_{\rm base}$ as a proxy and consider typical disk lens motion (relative to the bulge frame) $\boldsymbol{\mu} \sim (\mu_{\rm sgrA*}, 0)$, then this would predict $\mu_{\rm rel} \sim 5.6 + 6.4 \sim 12\,{\rm mas\,yr^{-1}}$. That is, a disk lens combined with the observed retrograde motion of the baseline object would naturally reproduce the relative proper motion derived from the lightcurve analysis.

Since the mass–distance constraint (Equation (4)) combined with upper limits on the lens flux already imply $D_{LS} \gtrsim 1.7\,{\rm kpc}$, and the measurements of $\mu_{\rm rel}$ and $\boldsymbol{\mu}_{\rm base}$ favor disk-lens kinematics, we conclude that the lens is almost certainly in the disk.

6. FUTURE MASS DETERMINATION

Because of the wide range of possible lens masses, we do not try to give a "best estimate. One could in principle attempt a Bayesian analysis based on a Galactic model, but this would require either assessing (or more likely ignoring) the priors on, e.g., an $M = 0.05\,M_\odot$ brown dwarf at $D_L = 1.6\,{\rm kpc}$ having an $m = 50\,M_\oplus$ planet at projected separation $r_\perp = 0.7\,{\rm AU}$ relative to an $M = 0.8\,M_\odot$ star at $D_L = 6.5\,{\rm kpc}$ having an $m = 3.8\,M_{\rm Jup}$ planet at $r_\perp = 3\,{\rm AU}$. Since this prior on relative planetary frequency is completely unconstrained, a Bayesian posterior estimate of the primary mass would essentially reflect the prior on the primary mass and therefore would not be informative.

Rather we focus on how the mass can be determined. First, one could measure the excess light (above the known flux from the source) in high-resolution images taken immediately. One limitation of this approach is that if the lens were even half as bright as the source then it would have been noticed already, and if it were less than a tenth as bright, it would be difficult to unambiguously detect. In addition, one must be concerned about nonlens stars generating the excess light, which could be either a random star along the line of sight or a companions to either the source or lens (e.g., Batista et al. 2014).

However, the high lens–source proper motion almost guarantees that this issue can be resolved by high-resolution imaging when the source and lens are separated by ∼100 mas, roughly 8 yr after the event, i.e., 2021. We note that while V. Batista et al. (2014, in preparation) have detected a planetary host lens separated from its source star by only 60 mas using Keck adaptive optics (AO), the source and lens fluxes were comparable in that case. In the present case, a lens at the bottom of the main sequence would be $H \sim 24$ and therefore roughly 100 times fainter than the source. Hence, to detect (or rule out) such a lens requires significantly greater separation. If the lens is not seen at that point, it must be "dark,which in practice means either a white dwarf at distance $D_L \sim 6\,{\rm kpc}$ or a brown dwarf at $D_L \lesssim 2.3\,{\rm kpc}$.

Note also that $\boldsymbol{\mu}_{\rm hel} - \boldsymbol{\mu}_{\rm geo} = \mathbf{v}_{\oplus,\perp}\pi_{\rm rel}/{\rm AU}$ where $\mathbf{v}_{\oplus,\perp} = (3.2, 6.6)\,{\rm km\,s^{-1}}$ is the velocity of Earth projected on the plane of the sky in equatorial coordinates (N, E). Therefore, if the lens is on the main sequence (and hence visible), then by Equation (1) $\pi_{\rm rel} < 0.3$, so that this correction to the proper motion is less than $0.5\,{\rm mas\,yr^{-1}}$.

7. CHARACTERIZATION USING ONLY FOLLOW-UP DATA

In the era of second-generation microlensing surveys, the relationship between survey and follow-up data is becoming more complex. From the standpoint of designing and implementing future strategies, it is important to establish the conditions under which planets can be characterized by survey-only data and by follow-up-only data, particularly for high-magnification events. For example, Yee et al. (2012) showed that although MOA-2011-BLG-293Lb was in practice discovered in follow-up data, it could have been well-characterized by survey data alone. Although Yee et al. (2012) did not explicitly address this question, the converse is not true: without survey data it would have been impossible to even approximately measure the event timescale $t_{\rm E}$ for that event. Similarly, Tsapras et al. (2014) investigated how well Poleski et al. (2014) had been able to characterize OGLE-2012-BLG-0406Lb based on survey-only data.

Here we ask the opposite question: how well can MOA-2013-BLG-220 be characterized by follow-up-only data? This may seem like a scholastic question, given that there are always survey data (because otherwise the event could not be "followed up"). However, already at present, on the order of 100 deg^2 are monitored at low cadence ($\lesssim$0.5 day^{-1}), and in the future many hundreds of square degrees may be monitored at even lower cadence (e.g., Gould 2013). These survey data may be too thin to provide any significant constraint on event characterization, and therefore they may be usefully approximated as being absent.

Because survey telescopes can switch into follow-up mode, it is not necessarily trivial to determine which observations should be assigned to each category. For example, in the case of MOA-2011-BLG-293, the cadence of OGLE data was greatly increased on the night of the anomaly alert relative to the normal cadence of $\sim$3 hr^{-1}. Yee et al. (2012) therefore approximated the "survey portion" as a subset following this cadence.

In the present case, we are fortunate that OGLE had to repoint the telescope in order to guarantee placement of the event on a chip. Thus we can reconstruct precisely, from the image headers, which OGLE observations are "follow-up. These turn out to be all observations $6386 < t < 6391$ and no others.

For MOA, the situation is more complicated. The cadence is much higher on the night of the second caustic entrance, which was in specific response to the alert. The decision to point the MOA telescope at this target for the single point on the cusp approach, which was observed earlier the same night during a momentary improvement in observing conditions, may have been strongly influenced by the alert as well. However, all of these points, whether considered "survey" or "follow-up," are closely matched by observations from the MOA B&C follow-up telescope operating from the same site, and all of the caustic-entrance points are covered by Turitea and Ellinbank as well. The one place where MOA data uniquely constrain the event is on the first caustic entrance. However, these took place before the alert and so are unquestionably "survey data." Hence, inclusion or exclusion of MOA follow-up data does not materially affect the follow-up-only fit. Therefore, for simplicity and to be conservative, we eliminate all MOA data from the follow-up-only analysis.

Table 2 shows the fit parameters resulting from models with only the follow-up data included. Comparison with Table 1 shows that all of the parameters are the same within errors and that the error bars themselves are only slightly larger.

Table 2
Parameters from Follow-up-Only Data

Parameter	Value	Error
$t_0 - 6386$	0.9197	0.0007
$u_0 \times 10^3$	13.20	0.05
$t_{\rm E}$ (days)	13.27	0.07
$\rho \times 10^3$	1.54	0.01
s	0.9857	0.0001
$q \times 10^3$	3.00	0.02
α (deg)	261.5	0.2
I_s (OGLE)	19.205	0.003
f_b/f_s (OGLE)	0.112	0.035
$\theta_{\rm E}$ (mas)[a]	0.456	0.003
$\mu_{\rm geo}$ (mas yr^{-1})[a]	12.52	0.08

Note. [a] Error shown is from lightcurve only. Additional 7% systematic error is discussed in the text.

8. DISCUSSION

This is the third event published in the era of survey-only microlensing planet detections (i.e., post-2010) in which follow-up observations play a decisive role, the other two being MOA-2011-BLG-293 and OGLE-2012-BLG-0026 (Han et al. 2013). We review the common features of these, which may be indicative of the role of follow-up observations in this era.

First, all three events were high-magnification. In such events, the planetary perturbations are often of shorter duration than in low-magnification events because the caustic is smaller. In addition, in contrast to low-magnification events, both the event characteristics and the planetary perturbation must be fit from the same peak data. Hence, these events benefit from the denser coverage that is made possible with follow-up. Also, the existence of multiple sites permits aggressive action in the face of weather or equipment problems at any given site.

Two of the events were in the wings of the season (early March and April, respectively), when pure-survey coverage is intrinsically limited and, again, aggressive multisite follow-up can compensate for the shortness of the observing night.

Finally, all three events were covered by CTIO-SMARTS, where H-band data are automatically taken using the dichroic ANDICAM camera (DePoy et al. 2003). As in the present case, the H-band data are usually not incorporated into the lightcurve analysis because they have much lower signal-to-noise ratio than the contemporaneous I/V data. However, these data proved crucial to the final interpretation of OGLE-2011-BLG-293Lb based on AO H-band observations taken a year after the event (Batista et al. 2014), and they are likely to prove crucial for MOA-2013-BLG-220Lb as well.

MOA issued its alert relatively early in the season when observations were possible only $\sim$5 hr per night. Given their 1.5 hr^{-1} cadence and variable conditions, this enabled three to five points per night. On the night of the μFUN alert, the event was already bright enough, and hence the photometric errors small enough, that the continued rise during the night was visible, which aided considerably in making the determination that the event was headed toward high magnification and so should be intensively observed. Hence, this is *not* an example of a call for high-cadence observations being issued on the basis of truly low-cadence survey data. For that, software of the type being developed by RoboNet would be necessary. Nevertheless, the fact that the planet could be characterized by follow-up observations alone shows that alerts derived from such low-cadence survey data (combined with automated moderate-cadence "patrols") can yield planet detections that are fully

characterized. This opens the prospect for complementing high-cadence surveys with very wide low-cadence surveys, when the latter are coupled to aggressive follow-up. Such a strategy could be employed over very wide ($\sim$6000 deg^2) areas using the Large Synoptic Survey Telescope (LSST) if that project does not exclude the inner two quadrants of the Galaxy (Gould 2013).

9. CONCLUSIONS

We have presented the discovery of a planet with relatively high mass ratio $q = 0.0030$, i.e., three times that of Jupiter and the Sun. The underlying event has a relatively high proper motion, 12.5 mas yr^{-1}. Two lines of argument show the planet lies in the Galactic disk. First, the measured Einstein radius $\theta_{\rm E} = 0.45$ mas, together with an upper limit on the lens flux, implies that the lens lies at least 1.7 kpc in front of the source. Second, the source (actually, "baseline object") proper motion is $\sim$6 mas yr^{-1} counter to Galactic rotation, implying that typical disk-lens motion of $\sim$6.5 mas yr^{-1} would naturally produce the observed lens–source relative proper motion. The actual lens mass and distance can be measured in the short term by looking for excess flux at the position of the lens in *Hubble Space Telescope* or ground-based AO observations provided it is at least 10% of the source brightness and otherwise by $\sim$2021, i.e., once the lens and source have moved far enough apart to be separately resolved.

Work by J. C. Yee is supported in part by a Distinguished University Fellowship from The Ohio State University and in part under contract with the California Institute of Technology (Caltech) funded by NASA through the Sagan Fellowship Program. Work by CH was supported by the Creative Research Initiative Program (2009-0081561) of the National Research Foundation of Korea. Work by A.G. and B.S.G. was supported by NSF grant AST 1103471. Work by A.G., B.S.G., and R.W.P. was supported by NASA grant NNX12AB99G. T.S. acknowledges the support from the grant JSPS23340044 and JSPS24253004. The OGLE project has received funding from the European Research Council under the European Community's Seventh Framework Programme (FP7/2007-2013)/ERC grant agreement no. 246678 to AU. This publication was made possible by NPRP grant X-019-1-006 from the Qatar National Research Fund (a member of Qatar Foundation).

REFERENCES

Alard, C., & Lupton, R. H. 1998, ApJ, 503, 325
Batista, V., Beaulieu, J.-P., Gould, A., et al. 2014, ApJ, 780, 54
Bennett, D. P., Rhie, S. H., Nikolaev, S., et al. 2010, ApJ, 713, 837
Bensby, T., Yee, J. C., Feltzing, S., et al. 2013, A&A, 549A, 147
Bessell, M. S., & Brett, J. M. 1988, PASP, 100, 1134
Bramich, D. 2008, MNRAS, 386, L77
Claret, A. 2000, A&A, 363, 1081
DePoy, D. L., Atwood, B., Belville, S. R., et al. 2003, Proc. SPIE, 4841, 827
Gaudi, B. S., Bennett, D. P., Udalski, A., et al. 2008, Sci, 319, 927
Gould, A. 1992, ApJ, 392, 442
Gould, A. 2004, ApJ, 606, 319
Gould, A. 2008, ApJ, 681, 1593
Gould, A. 2013, arXiv:1304.3455
Gould, A., & Gaucherel, C. 1997, ApJ, 477, 580
Gould, A., Udalski, A., Monard, B., et al. 2009, ApJL, 698, L147
Griest, K., & Safizadeh, N. 1998, ApJ, 500, 37
Han, C., Udalski, A., Choi, J.-Y., et al. 2013, ApJL, 762, L28
Hardy, S. J., & Walker, M. A. 1995, MNRAS, 276, L79
Kervella, P., Thévenin, F., Di Folco, E., & Ségransan, D. 2004, A&A, 426, 297
Nataf, D. M., Gould, A., Fouqué, P., et al. 2013, ApJ, 769, 88
Pejcha, O., & Heyrovský, D. 2009, ApJ, 690, 1772
Poleski, R., Udalski, A., Dong, S., et al. 2014, ApJ, 782, 48
Schechter, P. L., Mateo, M., & Saha, A. 1993, PASP, 105, 1342
Sumi, T., Kamiya, K., Bennett, D. P., et al. 2011, Natur, 473, 349
Tsapras, Y., Choi, J.-Y., Street, R. A., et al. 2014, ApJ, 782, 48
Yee, J. C., Shvartzvald, Y., Gal-Yam, A., et al. 2012, ApJ, 755, 102